HHS Public Access

Author manuscript

Magn Reson Med. Author manuscript; available in PMC 2019 January 01.

Published in final edited form as:

Magn Reson Med. 2018 January ; 79(1): 361–369. doi:10.1002/mrm.26695.

Regional Assessment of *In Vivo* Myocardial Stiffness Using 3D Magnetic Resonance Elastography in a Porcine Model of Myocardial Infarction

SP Arunachalam[1], **A Arani**[1], **F Baffour**[1], **JA Rysavy**[2], **PJ Rossman**[1], **KJ Glaser**[1], **DS Lake**[3], **JD Trzasko**[1], **A Manduca**[3], **KP McGee**[1], **RL Ehman**[1], and **PA Araoz**[1]

[1]Department of Radiology, Mayo Clinic, Rochester, MN

[2]Department of Surgery, Mayo Clinic, Rochester, MN

[3]Department of Physiology and Biomedical Engineering, Mayo Clinic, Rochester, MN

Abstract

Purpose—The stiffness of a myocardial infarct (MI) affects left ventricular (LV) pump function and remodeling. Magnetic Resonance Elastography (MRE) is a non-invasive imaging technique for measuring soft tissue stiffness *in vivo*. The purpose of this study was to investigate the feasibility of assessing *in vivo* regional myocardial stiffness with high frequency 3D cardiac MRE in a porcine model of myocardial infarction and compare the results with *ex vivo* uniaxial tensile testing.

Methods—MI was induced in a porcine model by embolizing the left circumflex artery. Fourteen days post-infarction, MRE imaging was performed in diastole using an ECG-gated spin-echo EPI sequence with 140 Hz vibrations and 3D MRE processing. MRE stiffness and tensile modulus from uniaxial testing were compared between remote and infarcted myocardium.

Results—Myocardial infarcts showed increased *in vivo* MRE stiffness compared to remote myocardium (4.6 ± 0.7 kPa vs. 3.0 ± 0.6 kPa, p = 0.02) within the same pig. *Ex vivo* uniaxial mechanical testing confirmed the *in vivo* MRE results, showing that myocardial infarcts were stiffer than remote myocardium (650 ± 80 kPa vs. 110 ± 20 kPa, p= 0.01).

Conclusions—These results demonstrate the feasibility of assessing *in vivo* regional myocardial stiffness with high frequency 3D cardiac MRE.

Keywords

Magnetic Resonance Elastography; myocardial infarction; myocardial stiffness; Heart Failure; cardiac MRE; Shear Modulus; cardiac elastography

Corresponding Author: Shivaram Poigai Arunachalam, Department of Radiology, Mayo Clinic, 200 First Street SW, Rochester, MN 55905; Phone: (507) 316-5839; Fax: (507) 284-9778; poigaiarunachalam.shivaram@mayo.edu.

INTRODUCTION

The stiffness of a myocardial infarct (MI) affects left ventricular (LV) pump function (1). Soft infarcts disrupt systolic function (2) and may be prone to rupture (3) while stiff infarcts impair diastolic filling (4). Infarct stiffness also affects the stress experienced by the remaining, non-infarcted myocardium, impacting ventricular function and remodeling (1). Because of this, infarct stiffness has been the target of therapies, such as injection of fibrin glue, to prevent LV remodeling and dilation associated with MI (5,6).

However, regional myocardial stiffness has not been directly measureable *in vivo* (7), with infarct stiffness historically being determined by *ex vivo* mechanical testing (8) (9) and more recently estimated with computational modeling (3). The inability to measure quantitative *in vivo* myocardial stiffness other than inferring from pressure-volume relationships has limited the use of stiffness as a prognostic tool, and may explain why there exists no means to predict infarct growth and remodeling that affects pump function (10). Therapies targeting infarct stiffness have had varying results, largely because results of therapy cannot be monitored *in vivo* nor applied to patients who might benefit most (3).

Magnetic Resonance Elastography (MRE) is a non-invasive imaging technique for measuring soft tissue stiffness *in vivo*. In MRE, target tissues are interrogated with shear waves from an external mechanical vibration source. The resulting propagating mechanical waves are imaged with a modified phase contrast magnetic resonance imaging (MRI) pulse sequence (11,12). Stiffness maps (called “elastograms”) are generated after application of one of a family of mathematical techniques, which are collectively referred to as “inversion.” MRE stiffness has been validated in phantoms, showing very high agreement with dynamic mechanical testing (intraclass correlation coefficient up to 0.99) (13). The technical feasibility of cardiac MRE has been previously described (9,14–16) (17,18), most recently using a high frequency *in vivo* 3D technique (19) where accuracy within 5 % at higher frequencies of vibration is achieved with isotropic voxels to accurately measure the 3D wave in all directions, 3D curl processing to remove the longitudinal component of the propagating shear wave, and adequate signal to prevent underestimation of stiffness which occurs when noisy regions are analyzed (13).

Recently, a low frequency (80 Hz) cardiac MRE technique was used to measure regional infarct stiffness in pigs (20); however, in that work the MRE acquisition was non-isotropic, the curl operator was not applied, and no metric of MRE signal was applied to ensure the reliability of the created stiffness maps. Therefore, the purpose of this study were (i) to perform regional assessment of *in vivo* myocardial stiffness with high frequency 3D cardiac MRE, using isotropic voxels, 3D curl processing and quantitative metrics of MRE signal quality, and (ii) to compare the results with *ex vivo* uniaxial tensile testing in a pig model of myocardial infarction.

MATERIALS AND METHODS

Animal Model

A porcine model was chosen for this study, and appropriate Institutional Animal Care and Use Committee (IACUC) approval was obtained. Seventeen pigs (male =10; female = 7) approximately 3 months old with average weight 49.4 ±2.3 kg were studied. Five pigs expired after creation of MI, prior to MRE imaging, and were excluded. Of the 12 surviving pigs, 7 had infarcts deemed too small to include in this study (described below), which left 5 pigs available for analysis.

Myocardial Infarct Creation

Myocardial infarction was induced using microsphere embolization of the left circumflex coronary artery. Telazol/Xylazine (5 mg/2mg per Kg) anesthesia was used in this study. Lidocaine and amiodarone anti-antiarrhythmic injections were used post-MI to sustain normal rhythms in the pigs, buprenorphine SR was used for post-operative pain management for the pigs, cephalexin antibiotic was used to protect the animals from infections, phenylephrine was used to maintain blood pressure and heparin anticoagulant was injected 10 minutes prior to injecting the KCl solution (21) for euthanasia. The pigs were intubated and placed under inhalational, general anesthesia, with continuous ECG monitoring. The pigs then received intravenous (IV) lidocaine (50 mg bolus) and/or a 100–150 mg IV bolus of amiodarone hydrocholoride over 15–20 minutes followed by 1mg/mL infusion at a rate of 30 mL/hr.

The microsphere embolization material was made up of 1–2 g of microspheres in 10 ccs of Saline and 2 ccs of contrast. After agitation to suspend the microspheres, they were injected slowly under fluoroscopic imaging until forward flow in the distal circumflex (distal to OM1) was stopped. A solution containing W-160 ceramic microspheres with 10 micron in diameter on an average (3M Inc., Maplewood, MN) and dilute contrast media was slowly injected at 5 and 15 minutes to verify that occlusion of the distal circumflex was complete. The catheter was then removed, the pig was monitored for another 45 minutes then the incision was closed and the pig was allowed to recover. A follow up MRI/MRE study was performed after 14 days, a time period associated with the onset of the fibrotic phase of myocardial infarction and increasing infarct stiffness in large animal models (1).

Magnetic Resonance Imaging/Elastography Image Acquisition

Fourteen days post-surgery, *in vivo* cardiac MRI was performed under inhalation anesthesia and mechanical ventilation. MRI imaging was performed with a 4-channel coil with two anterior and two posterior in a 1.5-Tesla MRI scanner (Signa Excite, GE Health Care, Milwaukee, WI). The experimental set up is illustrated in Figure 1. Pigs were positioned in prone position (feet first) with a custom-made MRE driver on the chest to maximize shear wave penetration for MRE imaging as previously described (19). ECG leads were placed on the back of the pig to ensure reliable ECG signal during motion vibration and the respiratory bellows was placed around the abdomen to monitor breath holds.

A cine balanced steady state free precession sequence (bSSFP) was used to acquire short-axis slices covering the entire left ventricle to measure LV volume, mass and wall motion (FOV =35 cm; resolution = 224×224, TR/TE 3.6/1.5, slice thickness = 5 mm; flip angle = 45, 20 cardiac phases, trigger window/delay (ms) = 35/10 with 20 slices). Late gadolinium enhancement (LGE) imaging was performed (FOV =35 cm; resolution = 224×160, TR/TE 6.5/3.2, slice thickness = 5 mm; flip angle = 20, NEX=2; 1 cardiac phase, trigger window/delay (ms) = 20/205 with 20 slices) after 2–3 minutes following infusion of a commercially available gadolinium-based contrast agent with 0.2 mmol/kg of gadodiamide (Omniscan, GE Healthcare Inc., Princeton, NJ) in the same short-axis plane prescribed by the bSSFP sequence so as to locate the infarct on MDE short-axis slices. The 2–3 minute time frame was selected as opposed to the 10 minute time frame used in human imaging because of the rapid circulation time of the pigs.

MRE Imaging was performed by prescribing slices to cover the infarct region as inferred from the MDE images using a modified ECG-gated spin-echo echo planar imaging sequence at 140 Hz vibration frequency with 5 breath holds of approximately 25 seconds each, depending on the heart rate, as previously described (19). A diastolic short-axis acquisition was performed prescribing time delays that corresponded to early diastole as observed from the bSSFP cine scan. The following acquisition parameters were used for this study: 1 shot, Number of Excitations (NEX) = 1; TR/TE = 4600/52ms; FOV = 28.8 cm; 96×96 image matrix; 11 continuous 3 mm thick slices, (resulting in a 3mm isotropic acquisition); 2 motion-encoding gradient (MEG) pairs on each side of the 180° RF pulse; x, y, and z motion-encoding directions; Parallel imaging using Sensitivity Encoding (SENSE) (22) reconstruction was accomplished using Array Spatial Sensitivity Encoding Technique (ASSET) with acceleration factor R = 2, and 4 phase offsets spaced evenly over one vibration period were used. Representative magnitude and wave images of the harmonic amplitudes are shown in Figure 2. A supporting video S1 showing the wave images is included.

To estimate shear wave quality, a “no-motion” scan was performed with the same parameters as above, with the vibration amplitude set to zero. This “no motion” scan was used to determine the level of MRE signal attributable to noise, and to exclude noisy regions as described in the “Magnetic Resonance Elastography Image Analysis” section below.

Pathological Analysis by Tri-phenyltetrazolium chloride (TTC) Staining

After MRE image acquisition, the pigs were sacrificed using potassium chloride (KCl) solution to arrest the heart in diastole that is known to preserve LV diastolic properties (21). The heart was then immediately excised and kept moist using a saline solution and was cut into short-axis sections. These short-axis myocardial slices were then stained with 2,3,5-triphenyltetrazolium chloride (TTC) to identify myocardial infarction (white) and remote myocardium (red).

Excluding Small Infarcts

As the goal of this study was to demonstrate the ability of MRE to measure stiffness in well-defined infarcts, only pigs with transmural infarcts encompassing greater than one

myocardial segment based on the AHA 17 segment model (23) on a short-axis, gross pathologic slice were included. Pigs with infarcts which did not meet these criteria were excluded from analysis. ST elevation was measured from ECG traces at the time of myocardial infarction. LV volumes, mass, and infarct size were measured with commercially available software (cmr42, Circle Cardiovascular Imaging, Calgary, Alberta) by manually tracing endocardial and epicardial contours on bSSFP images or manually tracing delayed enhancement regions on MDE images.

Mechanical Testing

The primary purpose of ex vivo tensile testing is to have an independent stiffness measurement to compare with MRE derived shear stiffness that will validate the relative stiffness difference between remote and infarcted myocardium, although shear stiffness and tensile modulus measure different properties of the tissue, and the experiments are carried out under very different conditions. Using anatomic landmarks, a short-axis pathologic slice that best approximated an MRI bSSFP and MDE short-axis slice demonstrating the infarct was selected for further analysis. Thin slices of infarcted and remote myocardial tissue were cut from the selected short-axis pathologic slices for mechanical testing within 1 hour post-mortem to avoid effects of rigor mortis on the tissue samples (24,25). Figure 3 A demonstrates tissue slicing from the short axis slice to obtain the remote and infarct samples used for mechanical testing. The average dimensions of the infarct samples across five samples were: 7.92 mm in thickness, 6.42 mm in depth and 35.72 mm long. Similarly the average dimensions of the remote samples across five samples were: 8.01 mm in thickness, 6.57 mm in depth and 37.15 mm long. Mechanical testing was a uniaxial tensile test performed with a MTS 858 Material Testing System (MTS Systems, EdenPraire, MN) as shown in Figure 3B. The gauge length, which is the grip to grip length, was set to 15mm for all the tests and the stretch rate was set at 1mm/sec displacement control. Strain was calculated as the difference between the grip to grip displacements observed from the uniaxial pulling towards sample destruction, and the gauge length. The samples were stretched towards destruction and stress was calculated by dividing the measured force in Newtons (N) divided by the area (mm^2) from the two width measurements after cutting the strips of muscle. Tensile modulus was then estimated as the slope (stress over strain in N/mm^2 or equivalent kPa) by performing linear regression in the linear portion of the curve for each sample. The experiment was performed in room temperature within 1 hour after excising the heart, which was kept in saline solution to keep it moist.

Magnetic Resonance Elastography Image Analysis

To generate MRE elastograms and quantify MRE stiffness, a 3D Local Frequency Estimation (LFE) inversion algorithm was applied as follows. First, the first temporal harmonic of the acquired wave images was calculated via temporal Fourier transform of the phase difference image series (3), and the curl operation was applied using a 6 nearest neighbor kernel to the complex 3D displacement field to remove the effects of longitudinal waves that would otherwise produce artifacts in the inversion results. Then, 3D LFE was performed on the curled first harmonic data to obtain the shear stiffness in kPa (26,27) using the standard default parameter settings for LFE (28). Shear stiffness was defined as the product of wave speed squared and density, where density was assumed to be that of water

(1,000 kg/m^3) as it is similar to the density of remote and infarcted myocardium. The left ventricle was semi-automatically segmented from the magnitude images using a random walker segmentation algorithm (29). Figure 4 shows a schematic of the MRE data processing steps that yield elastrograms from the wave images. For the purposes of this study, the myocardium (both remote and infarct) is assumed to be linearly elastic and isotropic, although the myocardium is known to be hyperelastic and anisotropic (1).

Gross pathology photographs, LGE images, and bSSFP cine images were used to localize the myocardial infarction. From these images a of region-of-interest (ROI) corresponding to the infarct location was drawn using FSL View Software on the MRE magnitude images while blinded to the elastograms. Eleven MRE slices were acquired and ROI's were drawn for the infarct in only those slices which best represented infarct location based on the reference pathology, LGE and bSSFP images. The ROIs were blindly copied from the magnitude image directly onto the elastogram to generate mean shear stiffness for remote myocardium and for infarcted myocardium (Figure 5). The vertical dimension of the infarct sample shown in Figure 3B is the circumferential direction in the short axis slice shown in Figure 5. Pixel-wise stiffness comparison was performed between the remote and the infarcted myocardium for each of the 5 pigs.

To assess shear wave quality within the ROIs and to exclude poor quality regions, a metric of shear wave quality was applied, namely the octahedral shear strain signal-to-noise ratio (OSS-SNR) (30). The "no motion" MRE acquisition, in which MRE images were obtained without any driver vibration, was used to determine the level of MRE signal attributable to noise and establish a minimum OSS-SNR threshold for ROIs to be included for analysis. For the 12 pigs in which MRE images had been obtained, the mean LV "no motion" OSS-SNR was measured. The mean and standard deviation of the "no motion" OSS-SNRs across the 12 pigs was calculated. The mean plus two times the standard deviation of the "no motion" OSS-SNR was set as the minimum required OSS-SNR for remote and infarct ROIs to be included for analysis.

Statistical Analysis

The characteristics of the 7 excluded and 5 included pigs were compared using a two-sided paired t-test in JMP statistical software (SAS Institute Inc., Cary, NC, 1989–2016). The remote and infarcted myocardial stiffness values from both MRE and tensile testing from the 5 included pigs were compared for statistical significance using Wilcoxon Signed Rank Test using Origin Pro software (OriginLab Corporation, Northampton, Massachusetts). A p-value of less than 0.05 was considered statistically significant. Statistical significance for pixel-wise stiffnesses for each of the the 5 pigs was tested between the remote and infarcted stiffness using Wilcoxon rank sum test. A p-value of less than 0.05 was considered statistically significant.

RESULTS

Of the surviving 12 pigs, 7 had infarcts that were non-transmural and/or smaller than a segment on the pathologic short-axis sections. The 5 remaining pigs were included in the analysis. The excluded pigs had very small infarcts (3.8 ± 3.2% of LV mass), which were

significantly smaller than the included pigs (9.0 ± 3.3%) (p = 0.01). The excluded pigs had minimal ST elevation (1.1 ± 1.1mm), which was less than that of the included pigs (3.7 ± 0.6mm) (p < 0.01). The characteristics of the 7 excluded and 5 included pigs are shown in Table 1.

The mean OSS-SNR for the 'no-motion" scans across the 12 pigs was 1.61±0.08. The mean plus two times standard deviation value for OSS-SNR for the "no-motion" scans was determined to be 1.77. This was therefore set as the threshold value for the scans with motion to be accepted for analysis. Each of the 5 pigs met this threshold for both the remote and infarcted myocardium (Figure 6) with a mean OSS-SNR of 1.97±0.19 for the remote myocardium and 2.65±0.75 for the infarcted myocardium. This ensured sufficient SNR for reliable estimates of shear stiffness within the included myocardial volume.

MRE stiffness of infarcted myocardium was higher than remote myocardium, with mean shear stiffness of the infarcted myocardium = 4.6 ± 0.7 kPa and the remote myocardium = 3.0 ± 0.6 kPa, p = 0.02. Figure 4 shows an example of the gross pathology image, magnitude and elastogram image from the same slice in Figure 2. MRE stiffness differences are plotted in Figure 7.

Ex vivo uniaxial mechanical testing showed that the infarcts were stiffer than the selected remote myocardium (p=0.01). The mean tensile modulus was 650 ± 80 kPa and 110 ±20 kPa for the infarct and remote myocardium, respectively (Figure 8), confirming the results of *in vivo* cardiac MRE.

Figure 9 shows the histogram of the pixel-wise stiffness for the remote and infarcted myocardium for each of the 5 pigs. The pixel-wise stiffness of the infarcted myocardium was significantly higher (p<0.0001) than the remote myocardium for each of the 5 pigs analyzed in this study.

Supporting figure S1 shows the correlation plot between MRE derived and tensile modulus infarct/remote stiffness ratio showing no significant relationship. Supporting figures S2–S6 shows the stress-strain curves for the 5 pigs analyzed in this study, for the remote and infarct myocardium where the slope of the linear fit is the estimated tensile modulus.

DISCUSSION

In this work we demonstrated, the feasibility of performing regional assessment of *in vivo* myocardial stiffness using high frequency 3D cardiac MRE. This paper is the first *in vivo* MRE paper to use isotropic voxels, 3D curl processing, and a quantitative metric of MRE signal in any cardiac application and only the second paper to attempt to measure regional differences in myocardial stiffness *in vivo*.

Only one paper, recently published by Mazumder et al., has attempted to measure regional MRE myocardial stiffness (20). The current work and the Mazumder study both showed increased MRE stiffness in myocardial infarcts, with similar absolute MRE values for infarcted and remote myocardium. The current study showed diastolic infarct MRE stiffness 4.6 ± 0.7 kPa compared to 5.09 ± 0.6 kPa for Mazumder et al. The current study showed

remote diastolic myocardium MRE stiffness of 3.0 ± 0.6 kPa compared to 3.97 ± 0.4 kPa for Mazumder et al. This similarity was seen even though there was a slight difference in the timing of infarct imaging. The current study imaged infarcts after 14 days, while Mazumder et al. imaged after 10 days. Mazumder et al also reported mean systolic stiffness of 5.72 ± 0.8 kPa 10 days post-MI and 6.34 ± 1.0 kPa 21 days post-MI for the infarcted myocardium compared to mean systolic stiffness of 5.08 ± 0.6 kPa for 10 days post-MI and 5.16 ± 0.6 kPa for 21 days post-MI for the remote myocardium. Also, our group has reported normal stiffness values at 140 Hz in systole (Arani et al, 2017) but not in diastole. Other studies have shown that systolic stiffness is higher than diastolic stiffness (Kolipaka et al, 2010) and the authors expect that the systolic stiffness at 140 Hz may be higher than the reported diastolic stiffness in this study.

There were also differences in the MRE technique. The current study imaged at a higher driving frequency (140 Hz), used isotropic (3mm) voxels, and applied 3D curl processing to remove the longitudinal component of the wave. Mazumder et al. imaged at a lower driving frequency (80 Hz), used non-isotropic pixels (8 × 3 × 3mm), and applied 2D band-pass filtering to partially remove thelongitudinal component of the wave. Future studies directly comparing the techniques in phantoms and *in vivo* may be helpful to determine the most clinically useful MRE technique.

To date, all other prior cardiac MRE work has only been attempted for global assessment of myocardial stiffness. Prior cardiac MRE studies have demonstrated increased myocardial stiffness in systole compared to diastole in both animal models (14) and humans and also under different loading conditions in animals (15). Transthoracic time-harmonic shear wave amplitudes at low-vibration frequency have been used to estimate myocardial stiffness (17); however, this approach does not generate elastograms and regional assessment of stiffness has not been demonstrated with this technique.

This study is the first cardiac MRE study to use quantitative shear wave quality metrics as a requirement for inclusion. Prior cardiac MRE studies have used non-quantitative, visual assessment of waves (16) or did not exclude samples based on noise (20). Poor wave propagation can lead to noisy images, which in turn cause inversion algorithms to underestimate stiffness (31–34). This can be problematic when, as in our study and the study by Mazumder et al. the infarct regions consistently occur in same region and could systematically experience different amplitude waves than the remote regions.

The OSS-SNR is very dependent on imaging parameters (particularly voxel size) and inversion algorithm and for that reason the threshold we used differs from thresholds previously reported prior studies and is specific to this application. The strain SNR is affected by both the imaging parameters especially the spatial resolution which decreases with higher resolution and longer wavelengths (30). That is why the OSS-SNR threshold used here (1.77) does not match the OSS-SNR threshold of 3.0 described in the original report of OSS-SNR by McGarry et al. McGarry’s application used isotropic voxels of 2.0 mm (as opposed to 3.0 in our application) and used a finite-element based inversion algorithms (30), as opposed to LFE as in the current study. Our threshold is also slightly different than the 1.6 threshold previously reported by our group in a study of normal

volunteers as the voxel size was different from that study and the current study. In the future, new MRE metrics should be developed which are independent of imaging parameters and inversion, to allow for uniform standards across different MRE applications.

There are several limitations in this study. First, only pigs with larger infarcts were included in this study, though the included infarcts were still only about 9 % of the LV mass, a size which would still be characterized as “small” in prior MRI studies of myocardium infarction (2) (35). The excluded pigs had extremely small infarcts (non-transmural and average size of 3.8% of LV mass) a size frequently not detectable by nuclear myocardial perfusion scanning (36–38). Also, we estimated infarct location and drew the ROI’s blinded to the elastogram from gross pathology, bSSFP and LGE images which did not exactly match MRE magnitude images. There was a concern that misregistration could cause partial of complete exclusion of the small infarcts from the ROI’s resulting in inaccurate MRE stiffness for the small infarcts. As the goal of this study was to demonstrate the initial feasibility of regional assessment of 3D cardiac MRE, it was decided to only include larger infarcts. The prior study by Mazumder et al. did not report infarct size for comparison with our study, and the authors chose to include only larger infarcts for analysis in this study as discussed above. Future studies will be necessary to determine the sensitivity of cardiac MRE for detecting very small infarcts.

Secondly, the mechanical testing approach used in this study is not directly comparable to the MRE measurement for several reasons. The mechanical testing measures tensile modulus, which is not the same quantity as the shear stiffness measured by MRE. The MRE measurement is at 140 Hz, while the mechanical testing is essentially at DC. The measurements probe different regions of the stress-strain curves shown in supporting figures S2–S6: MRE operates at strain levels of ~0.1%, while the mechanical testing fits varied but were typically in the 20–60% strain range, where hyperelastic material properties may be relevant. The myocardium is anisotropic, and there was no control of the relationship between wave propagation and fiber direction in MRE, or of the direction chosen for uniaxial testing. Finally, the mechanical testing is an *ex vivo* measurement, while the MRE measurement is *in vivo*, which introduces additional differences between the measurements. All of these factors likely contribute to the large absolute differences between the MRE and mechanical testing results.

There are several existing methods for determing regional myocardial stiffness *in vivo* such as pressure-length relationships (1). Other investigators have used simultaneous pressure measurements accompanied by strain and combined with finite element methods (FEM) to estimate stiffness (39–40). However, *ex vivo* mechanical testing though imperfect, is well established for determining relative differences in myocardial stiffness within the same animal (1). Moreover the uniaxial testing was performed within an hour post-mortem which has been previously shown not to affect the testing results due to rigor mortis (24,25). Also, in this study euthanasia was performed with KCl, which arrests the heart in diastole (21) allowing for optimal comparison since the MRE scans, which were performed in diastole.

The authors observed no significant correlation between the MRE derived stiffness and mechanical testing derived tensile modulus in this study, with highhigh inter-pig variability.

However, comparison within the same pig can eliminate some variability and can be more meaningful for comparison purposes. The ratio of the mean infarct to remote myocardial stiffness from tensile testing is approximately 6 compared to 2 for MRE derived stiffness. As seen in supporting figure S1, there was no significant correlation between MRE derived and tensile modulus infarct/remote stiffness ratios. These large differences could be attributed to the factors mentioned above, as well as the 10–15% pre-compression force necessary to hold the tissue samples for uniaxial testing (and the difficulty of controlling this force), the fact that slipping was sometimes observed between the sample and the grip in the initial stages of stretching, and the possibility of obtaining infarct and remote samples with different fiber direction across different animals. Similar lack of significant correlation between MRE derived and mechanical testing derived stiffness has been reported before (Kolipaka et al.). Future animal studies will focus on performing test retest repeatability approaches to fine tune the stiffness estimation from mechanical testing to have a more reasonable comparison with MRE derived stiffness.

Finally, myocardial infarcts can be highly anisotropic in some cases and isotropic in others (3), while normal myocardium is always anisotropic and the myocardial fibers change their orientation between endocardium and epicardium (7). The LFE inversion algorithm used in this study assumes an isotropic material with local homogeneity (26) (31). Anisotropic inversions have been described in a few reports in neurological applications (41), but these techniques are not currently feasible in the heart. Future cardiac MRE applications may be developed which account for myocardial anisotropy; however, they are beyond the scope of this work.

CONCLUSIONS

This work has demonstrated the feasibility of 3D cardiac MRE to estimate *in vivo* differences in myocardial stiffness between remote and infarct regions in a pig model with induced myocardial infarction. Both MRE and mechanical testing found infarcts to be significantly stiffer than remote myocardium. Future work will focus on determining the prognostic significance of cardiac MRE infarct stiffness measurements.

Supplementary Material

Refer to Web version on PubMed Central for supplementary material.

Acknowledgments

The authors would like to thank Mr. Berglund Lawrence, Biomechanics Testing Laboratory, Mayo Clinic, Rochester, MN for performing the uniaxial testing of the tissue samples for this study. This study was supported by National Institute of Health (NIH) grants 5R01HL115144 and EB001981.

References

1. Holmes JW, Borg TK, Covell JW. Structure and mechanics of healing myocardial infarcts. Annu Rev Biomed Eng. 2005; 7:223–53. [PubMed: 16004571]
2. Bogen DK, Rabinowitz SA, Needleman A, McMahon TA, Abelmann WH. An analysis of the mechanical disadvantage of myocardial infarction in the canine left ventricle. Circ Res. 1980; 47:728–41. [PubMed: 7418131]

3. Clarke SA, Richardson WJ, Holmes JW. Modifying the mechanics of healing infarcts: Is better the enemy of good? J Mol Cell Cardiol. 2016; 93:115–24. [PubMed: 26631496]

4. Holmes JW, Nunez JA, Covell JW. Functional implications of myocardial scar structure. Am J Physiol. 1997; 272:H2123–30. [PubMed: 9176277]

5. Christman KL, Lee RJ. Biomaterials for the treatment of myocardial infarction. J Am Coll Cardiol. 2006; 48:907–13. [PubMed: 16949479]

6. Leor J, Tuvia S, Guetta V, et al. Intracoronary injection of in situ forming alginate hydrogel reverses left ventricular remodeling after myocardial infarction in Swine. J Am Coll Cardiol. 2009; 54:1014–23. [PubMed: 19729119]

7. Kurnik PB, Michael R. Courtois, and Philip A. Ludbrook. Left ventricular myocardial stiffness. Mathematical and Computer Modelling. 1988; 11:5.

8. Mirsky I, Parmley WW. Assessment of passive elastic stiffness for isolated heart muscle and the intact heart. Circ Res. 1973; 33:233–43. [PubMed: 4269516]

9. Kolipaka A, Aggarwal SR, McGee KP, et al. Magnetic resonance elastography as a method to estimate myocardial contractility. J Magn Reson Imaging. 2012; 36:120–7. [PubMed: 22334349]

10. Gao XM, White DA, Dart AM, Du XJ. Post-infarct cardiac rupture: recent insights on pathogenesis and therapeutic interventions. Pharmacol Ther. 2012; 134:156–79. [PubMed: 22260952]

11. Muthupillai R, Lomas DJ, Rossman PJ, Greenleaf JF, Manduca A, Ehman RL. Magnetic resonance elastography by direct visualization of propagating acoustic strain waves. Science. 1995; 269:1854–7. [PubMed: 7569924]

12. Muthupillai R, Ehman RL. Magnetic resonance elastography. Nat Med. 1996; 2:601–3. [PubMed: 8616724]

13. Arunachalam SP, Rossman PJ, Arani A, et al. Quantitative 3D magnetic resonance elastography: Comparison with dynamic mechanical analysis. Magn Reson Med. 2017 Mar; 77(3):1184–1192. [PubMed: 27016276]

14. Kolipaka A, Araoz PA, McGee KP, Manduca A, Ehman RL. Magnetic resonance elastography as a method for the assessment of effective myocardial stiffness throughout the cardiac cycle. Magn Reson Med. 2010; 64:862–70. [PubMed: 20578052]

15. Kolipaka A, McGee KP, Manduca A, Anavekar N, Ehman RL, Araoz PA. In vivo assessment of MR elastography-derived effective end-diastolic myocardial stiffness under different loading conditions. J Magn Reson Imaging. 2011; 33:1224–8. [PubMed: 21509882]

16. Wassenaar PA, Eleswarpu CN, Schroeder SA, et al. Measuring age-dependent myocardial stiffness across the cardiac cycle using MR elastography: A reproducibility study. Magn Reson Med. 2016; 75:1586–93. [PubMed: 26010456]

17. Elgeti T, Knebel F, Hattasch R, Hamm B, Braun J, Sack I. Shear-wave amplitudes measured with cardiac MR elastography for diagnosis of diastolic dysfunction. Radiology. 2014; 271:681–7. [PubMed: 24475861]

18. Sack I, Rump J, Elgeti T, Samani A, Braun J. MR elastography of the human heart: noninvasive assessment of myocardial elasticity changes by shear wave amplitude variations. Magn Reson Med. 2009; 61:668–77. [PubMed: 19097236]

19. Arani A, Glaser KL, Arunachalam SP, et al. In vivo, high-frequency three-dimensional cardiac MR elastography: Feasibility in normal volunteers. Magn Reson Med. 2017 Jan; 77(1):351–360. [PubMed: 26778442]

20. Mazumder R, Schroeder S, Mo X, et al. In vivo magnetic resonance elastography to estimate left ventricular stiffness in a myocardial infarction induced porcine model. J Magn Reson Imaging. 2016

21. Rabkin DG, Jia CX, Cabreriza SE, Hart JP, Starr JP, Spotnitz HM. A novel arresting solution for study of postmortem pressure–volume curves of the rat left ventricle. J Surg Res. 1998; 80:221–8. [PubMed: 9878317]

22. Pruessmann KP, Weiger M, Scheidegger MB, Boesiger P. SENSE: sensitivity encoding for fast MRI. Magnetic resonance in medicine. 1999; 42(5):952–962. [PubMed: 10542355]

23. Cerqueira MD, Weissman NJ, Dilsizian V, et al. Standardized myocardial segmentation and nomenclature for tomographic imaging of the heart. A statement for healthcare professionals from

the Cardiac Imaging Committee of the Council on Clinical Cardiology of the American Heart Association. Circulation. 2002; 105:539–42. [PubMed: 11815441]

24. Van Ee CA, Chasse AL, Myers BS. Quantifying skeletal muscle properties in cadaveric test specimens: effects of mechanical loading, postmortem time, and freezer storage. J Biomech Eng. 2000; 122:9–14. [PubMed: 10790824]
25. Morrow DA, O GM, Kaufman KR. Use of a Poroelastic Model to Predict Intramuscular Pressure. Poromechanics V: proceedings of the fifth Biot Conference on Poromechanics. 2013; 2013:2174–2183. [PubMed: 25541627]
26. Manduca A, Muthupillai R, Rossman PJ, Greenleaf JF, Ehman RL. Local wavelength estimation for magnetic resonance elastography. Image Processing, 1996 Proceedings, International Conference. 1996; 3:527–530.
27. Manduca A, Oliphant TE, Dresner MA, et al. Magnetic resonance elastography: non-invasive mapping of tissue elasticity. Medical image analysis. 2001; 5:237–54. [PubMed: 11731304]
28. Grimm, RC., D, L., Manduca, A., Ehman, RL. MRE/Wave. Rochester (MN): Mayo Clinic; 2006. [updated 2006 July 1; cited ____]. Available from http://mayoresearchmayoedu/mayo/research/ehman_lab
29. Grady L. Random walks for image segmentation. IEEE Trans Pattern Anal Mach Intell. 2006; 28:1768–83. [PubMed: 17063682]
30. McGarry MD, Van Houten EE, Perrinez PR, Pattison AJ, Weaver JB, Paulsen KD. An octahedral shear strain-based measure of SNR for 3D MR elastography. Phys Med Biol. 2011; 56:N153–64. [PubMed: 21654044]
31. Manduca A, Oliphant TE, Dresner MA, Mahowald JL, Kruse SA, Amromin E, Felmlee JP, Greenleaf JF, Ehman RL. Magnetic resonance elastography: non-invasive mapping of tissue elasticity. Medical image analysis. 2001; 5(4):237–254. [PubMed: 11731304]
32. Manduca A, Oliphant TE, Dresner MA, Lake DS, Greenleaf JF, Ehman RL. Comparative evaluation of inversion algorithms for magnetic resonance elastography. Proceedings - International Symposium on Biomedical Imaging IEEE Computer Society. 2002:997–1000.
33. Sinkus R, Tanter M, Xydeas T, Catheline S, Bercoff J, Fink M. Viscoelastic shear properties of in vivo breast lesions measured by MR elastography. Magnetic resonance imaging. 2005; 23(2):159–165. [PubMed: 15833607]
34. Sinkus R, Tanter M, Catheline S, et al. Imaging anisotropic and viscous properties of breast tissue by magnetic resonance-elastography. Magn Reson Med. 2005; 53:372–87. [PubMed: 15678538]
35. Gjesdal O, Helle-Valle T, Hopp E, et al. Noninvasive separation of large, medium, and small myocardial infarcts in survivors of reperfused ST-elevation myocardial infarction: a comprehensive tissue Doppler and speckle-tracking echocardiography study. Circ Cardiovasc Imaging. 2008; 1:189–96. 2 p following 196. [PubMed: 19808542]
36. Lee VS, Resnick D, Tiu SS, et al. MR imaging evaluation of myocardial viability in the setting of equivocal SPECT results with (99m)Tc sestamibi. Radiology. 2004; 230:191–7. [PubMed: 14617765]
37. Lund GK, Stork A, Saeed M, et al. Acute myocardial infarction: evaluation with first-pass enhancement and delayed enhancement MR imaging compared with 201Tl SPECT imaging. Radiology. 2004; 232:49–57. [PubMed: 15166320]
38. Wagner A, Mahrholdt H, Holly TA, et al. Contrast-enhanced MRI and routine single photon emission computed tomography (SPECT) perfusion imaging for detection of subendocardial myocardial infarcts: an imaging study. Lancet. 2003; 361:374–9. [PubMed: 12573373]
39. Haraldsson H, Hope M, Acevedo-Bolton G, Tseng E, Zhong X, Epstein FH, Ge L, Saloner D. Feasibility of asymmetric stretch assessment in the ascending aortic wall with DENSE cardiovascular magnetic resonance. Journal of Cardiovascular Magnetic Resonance. 2014; 16(1):6. [PubMed: 24400865]
40. Sun K, Stander N, Jhun CS, Zhang Z, Suzuki T, Wang GY, Saeed M, Wallace AW, Tseng EE, Baker AJ, Saloner D. A computationally efficient formal optimization of regional myocardial contractility in a sheep with left ventricular aneurysm. Journal of biomechanical engineering. 2009; 131(11):111001. [PubMed: 20016753]

41. Romano A, Guo J, Prokscha T, et al. In vivo waveguide elastography: effects of neurodegeneration in patients with amyotrophic lateral sclerosis. Magn Reson Med. 2014; 72:1755–61. [PubMed: 24347290]

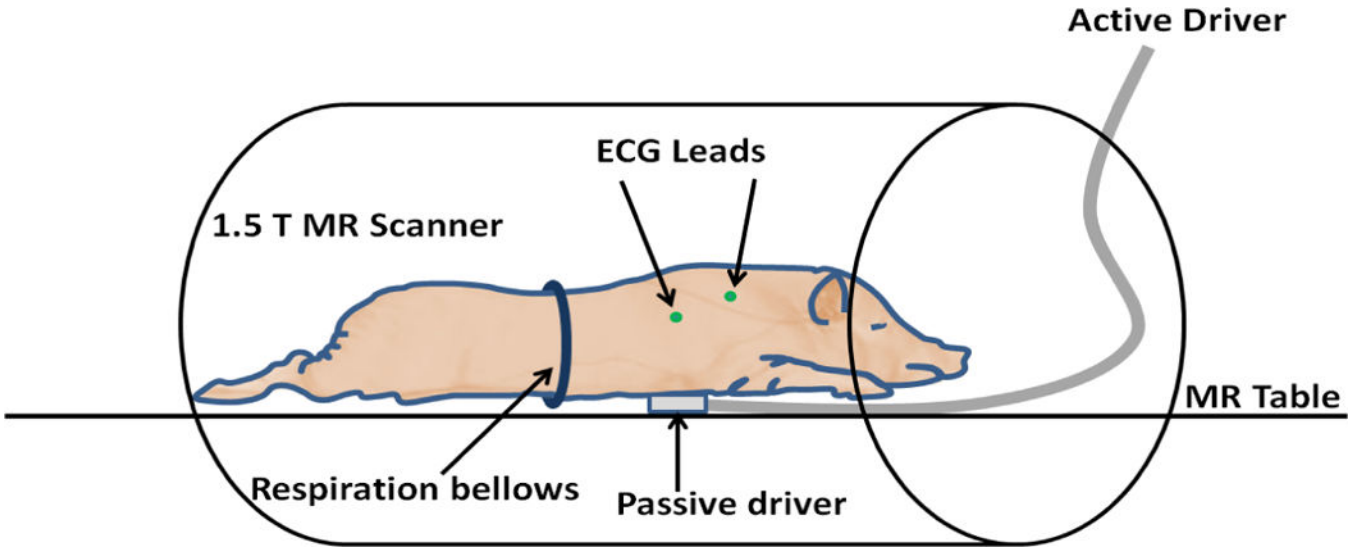

Figure 1.
Experimental setup of the pig model with MRE passive driver on the chest in prone position.

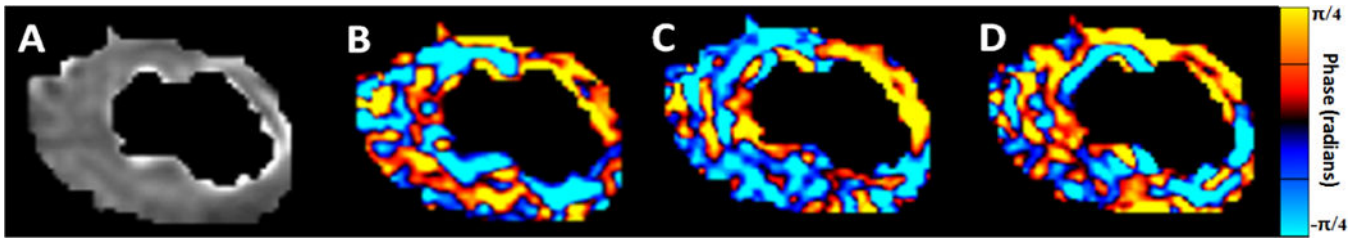

Figure 2.

This figure shows a representative example from a pig. (A) Magnitude image of a short-axis slice after LV masking (B) Corresponding X-component of the curled image (C) Corresponding Y-component of the curled image (D) Corresponding Z-component of the curled wave field.

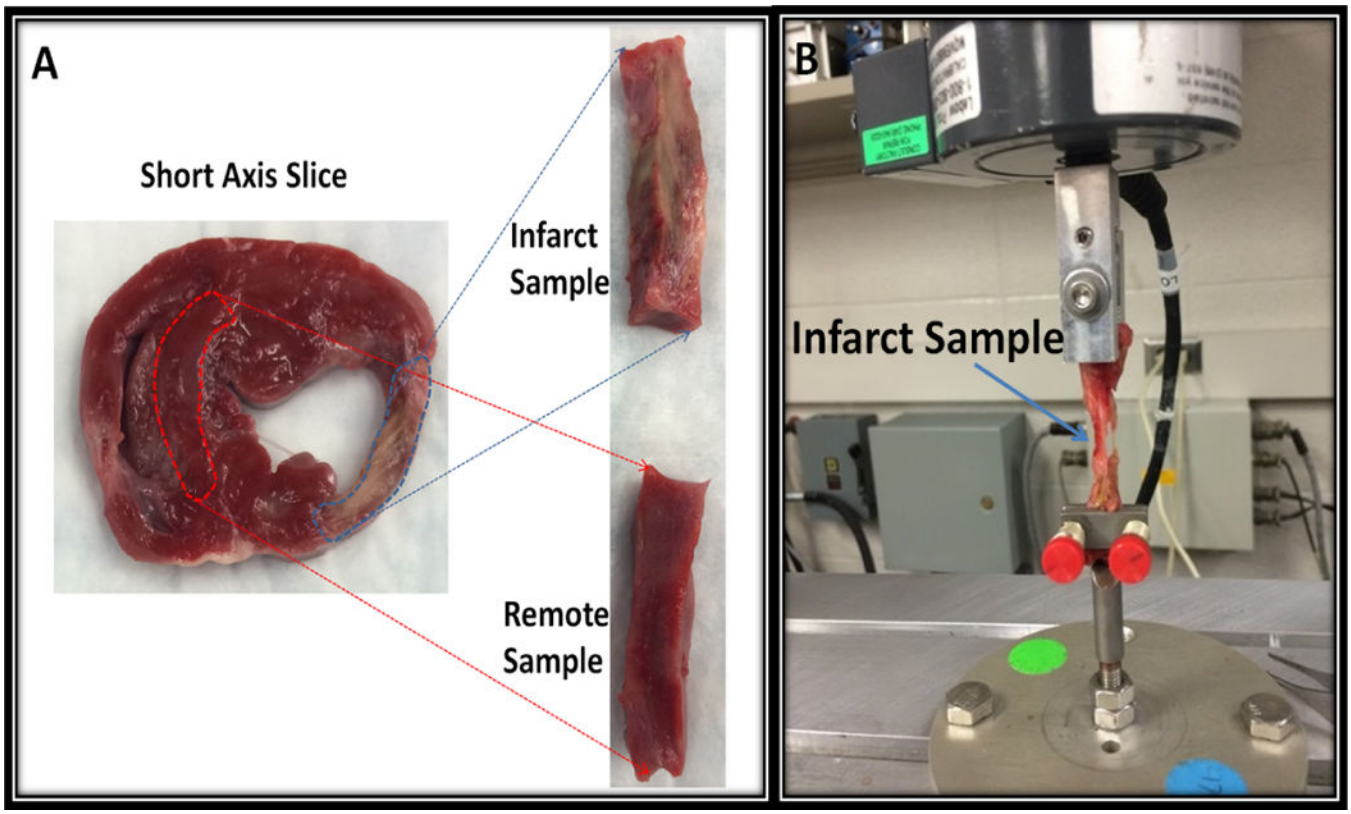

Figure 3.

(A): Figure demonstrating sample preparation from short axis gross tissues for mechanical testing (B): Material Testing System performing uniaxial tensile test on an infarct sample being stretched towards destruction.

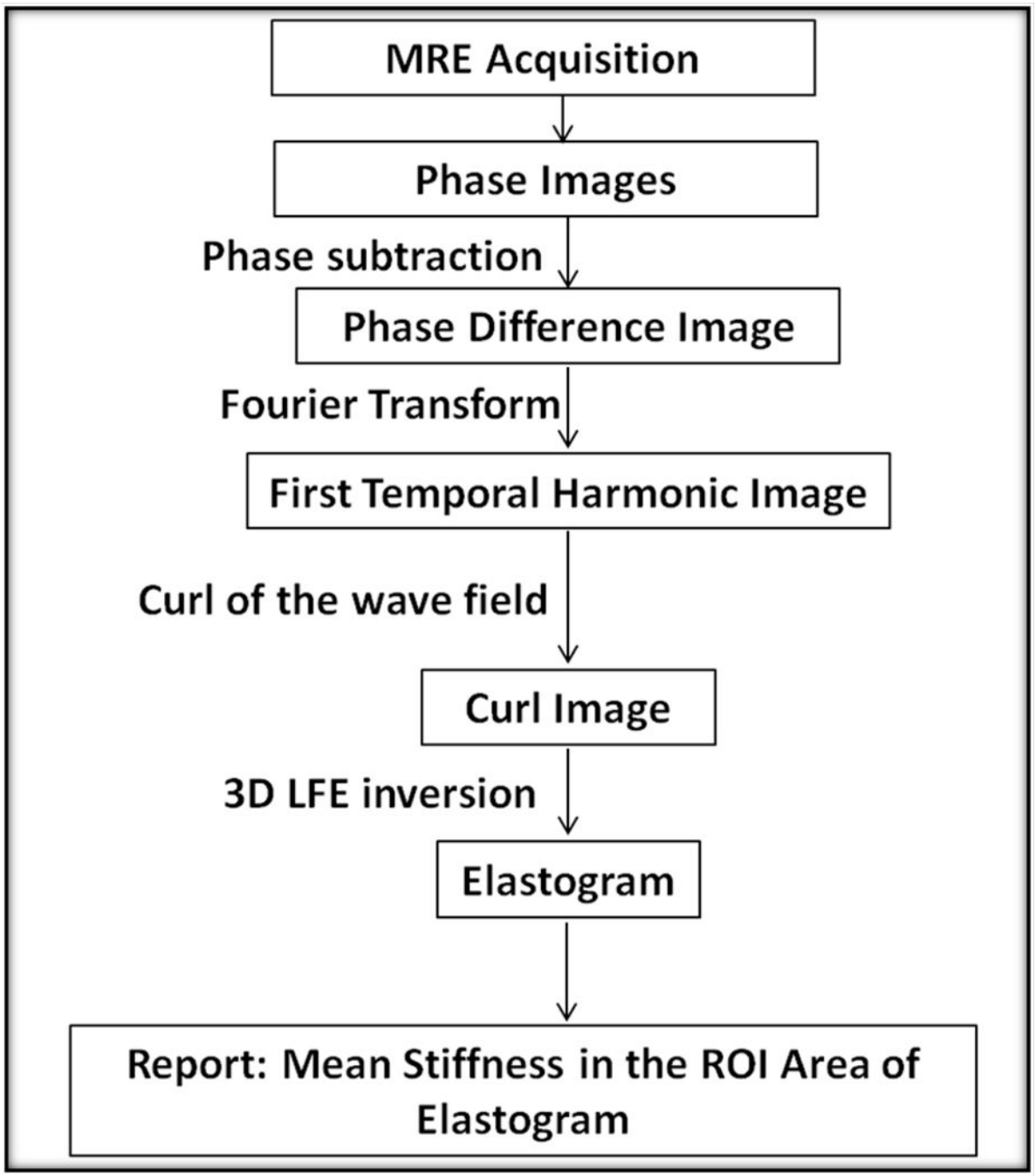

Figure 4.

MRE Inversion flow chart. MRE acquired images are converted into elastograms through multiple steps, including applying the curl operator to the first temporal harmonic image. Regions of interest are drawn onto magnitude image and copied onto the elastogram. The curl images are also used to generate OSS-SNR maps on the 140 Hz and the no-motion images.

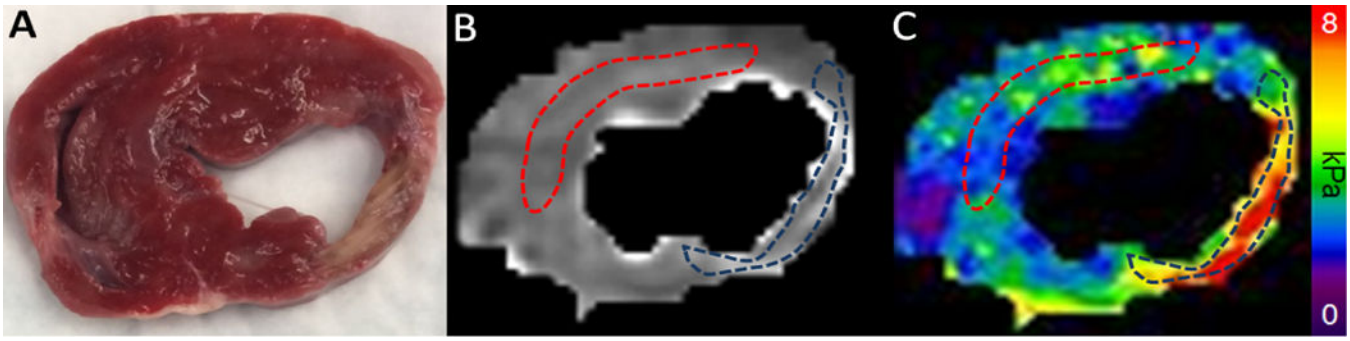

Figure 5.

Image Analysis. (A) Pathology image showing the infarct in a short-axis slice. Using the pathology image, delayed enhancement, and cine balanced Steady State Free Precession (bSSFP) cine images, a region-of-interest (ROI) was drawn onto (B) the magnitude image from the MRE acquisition, blinded to the wave images and to the elastogram. Infarct is indicated by the dark ROI and remote tissue by red ROI. These ROIs were copied onto (C) the elastogram image corresponding to the magnitude image and from these ROIs the mean MRE stiffness for remote and infarcted myocardium was calculated.

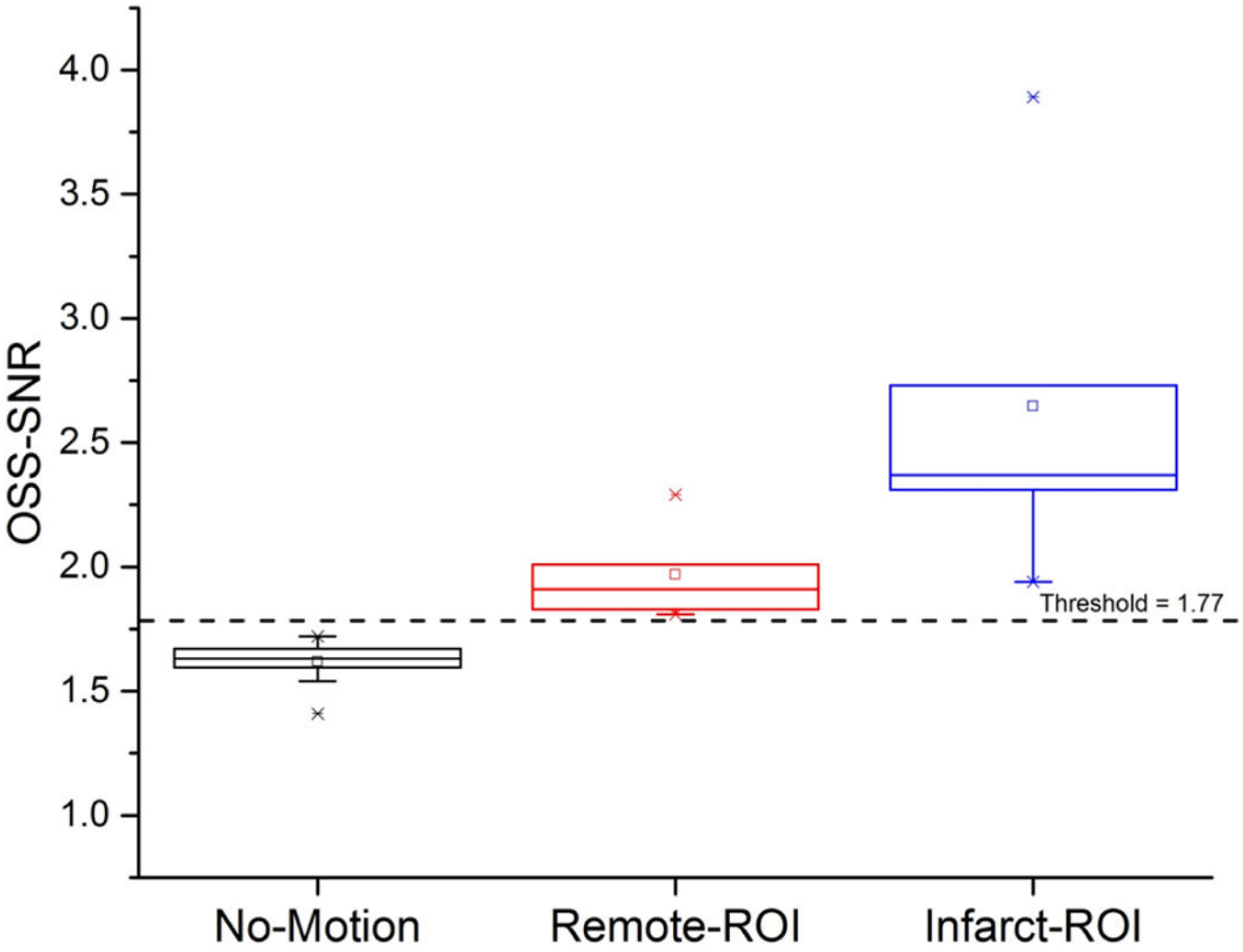

Figure 6.

Box-plot of OSS-SNR mean values for the no-motion scans for the segmented left ventricles of all 12 pigs which underwent cardiac MRE, infarct and remote myocardial regions-of-interest (ROI) at 140 Hz vibrations. The black dotted line represents the threshold value of OSS-SNR of 1.77 (mean plus two standard deviations of the no-motion scans) used to distinguish motion signal from noise.

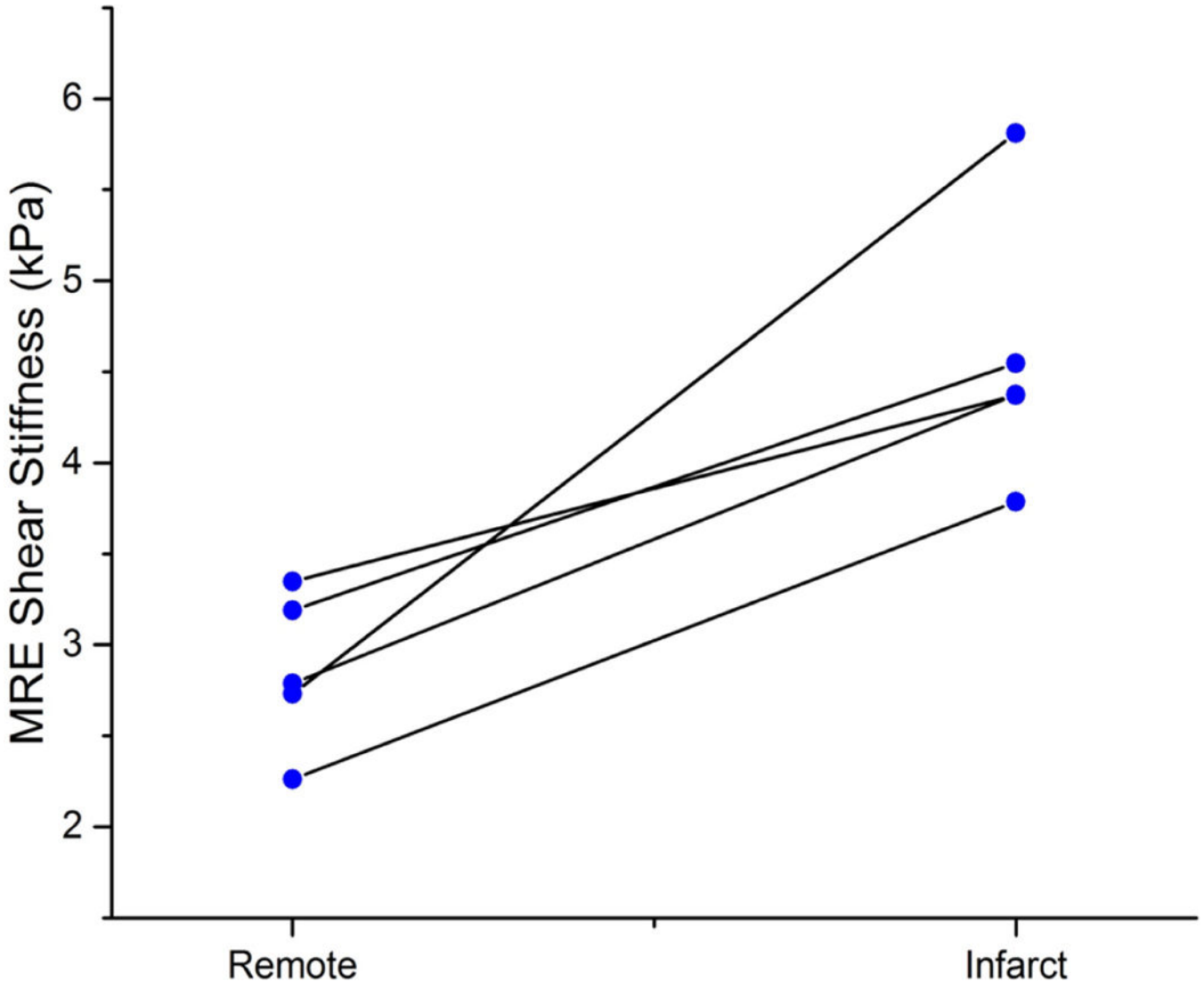

Figure 7.

Paired- plot of infarct and remote myocardium MRE shear stiffness. Infarcted myocardial stiffness is significantly higher than the remote myocardial stiffness with p =0.02.

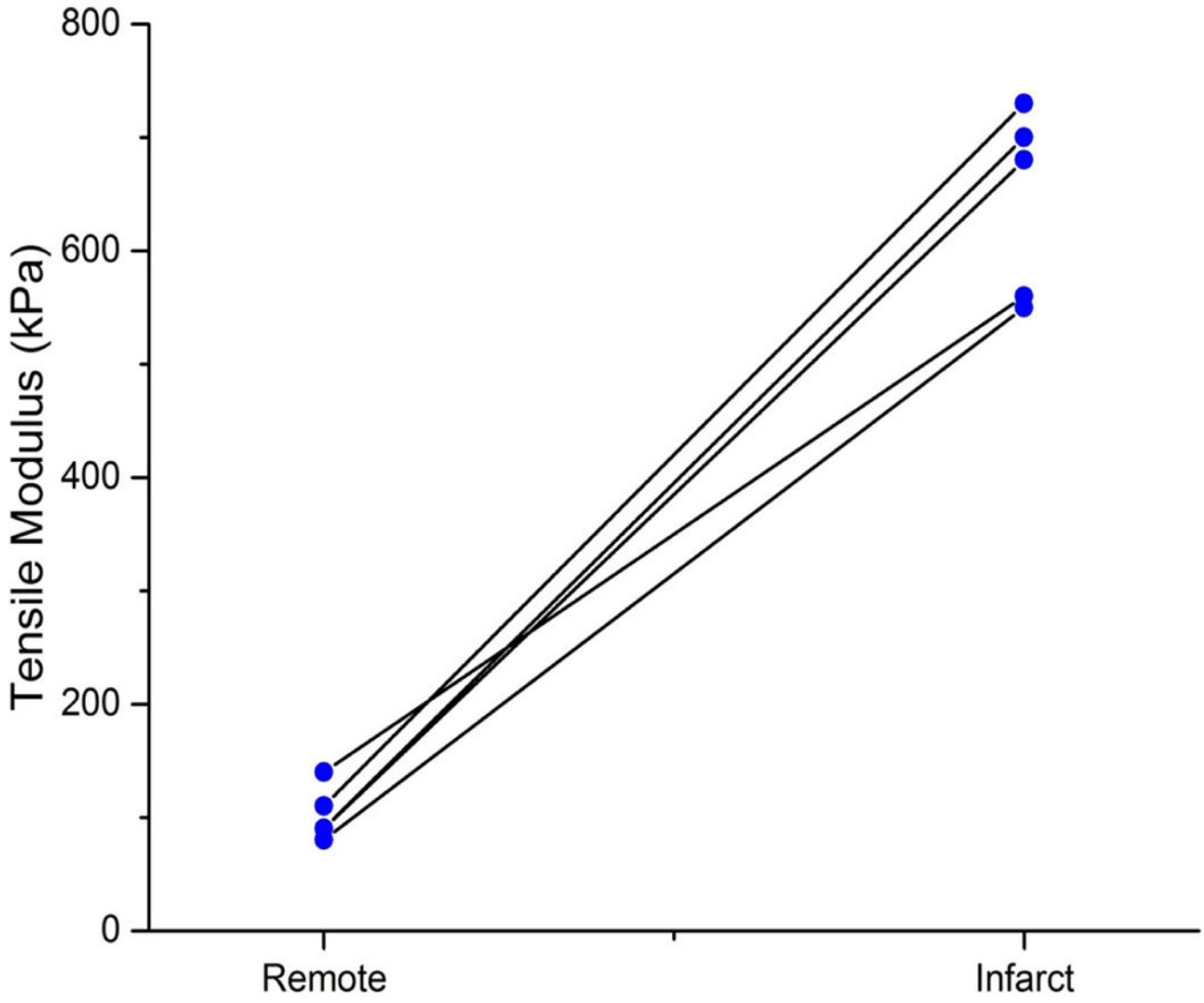

Figure 8.

Paired-plot of infarct and remote myocardium tensile modulus from uniaxial tensile testing. Infarcted myocardial tensile modulus is significantly higher than the remote myocardial tensile modulus with p =0.01.

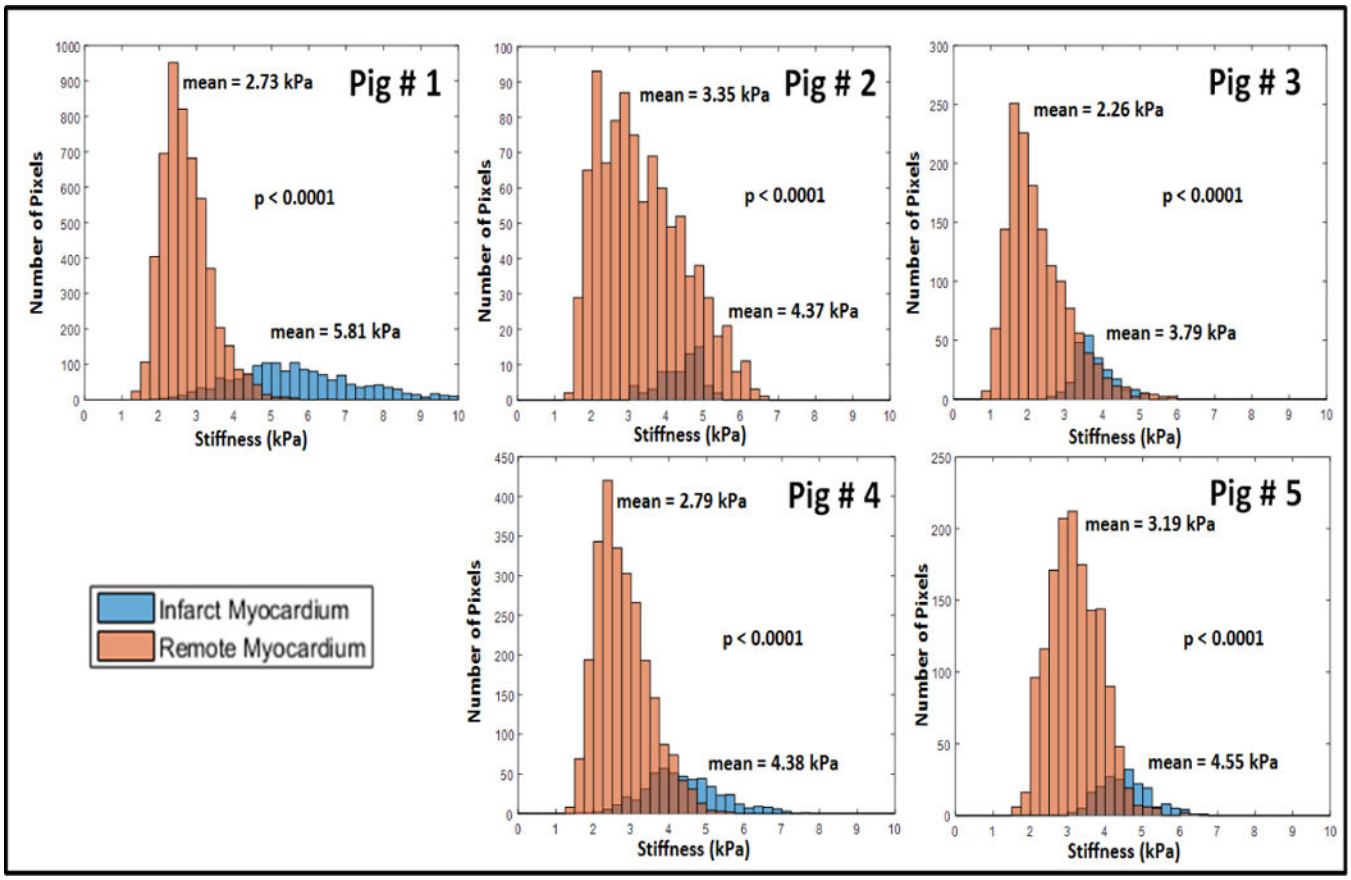

Figure 9.

Histogram of pixel-wise stiffness estimates for the infarct and remote ROI's used for the five different pigs analyzed in this study. X-axis shows the stiffness (kPa) and Y-axis represents number of pixels. The mean values of the remote and infarct stiffness are reported near the corresponding histograms. Infarcted myocardium was significantly stiffer ($p < 0.0001$) than the remote myocardium in each of the 5 pigs. There are more pixels for the remote ROI as the infarct ROI's were relatively smaller.

Table 1

Table 1 shows various measurements such as ST elevation (mm), left ventricle (LV) infarct size (%), LV mass (g), left ventricular end-diastolic volume (LVEDV) (mL), left ventricular end-systolic volume (LVESV) (mL), left ventricular stroke volume (LVSV) (mL) and left ventricular ejection fraction (LVEF) (%).

Parameter	Pigs included in analysis (n = 5)	Pigs excluded from analysis (n = 7)	P value
ST elevation (mm)	3.7 ± 0.6	1.1 ± 1.1	< 0.01
LV infarct size (%)	9.0 ± 3.3	3.8 ± 3.2	0.01
LV mass (g)	123.2 ± 10.5	104.3 ± 8.4	<0.01
LVEDV (mL)	88.0 ± 12.3	79.6 ± 17.0	0.36
LVESV (mL)	51.4 ± 15.2	40.7 ± 13.8	0.23
LVSV (mL)	36.6 ± 4.6	40.3 ± 8.3	0.39
LVEF (%)	42.8 ± 9.2	49.7 ± 8.0	0.19